Switching Colloidal Superstructures by Critical Casimir Forces

Nguyen, T.A.; Newton, A.; Veen, S.J.; Kraft, D.J.; Bolhuis, P.G.; Schall, P.

DOI
10.1002/adma.201700819

Publication date
2017

Document Version
Final published version

Published in
Advanced materials

ADVANCED MATERIALS
www.advmat.de

Switching Colloidal Superstructures by Critical Casimir Forces

*Truc A. Nguyen, Arthur Newton, Sandra J. Veen, Daniela J. Kraft, Peter G. Bolhuis, and Peter Schall**

Recent breakthroughs in colloidal synthesis promise the bottom-up assembly of superstructures on nano- and micrometer length scales, offering molecular analogues on the colloidal scale. However, a structural control similar to that in supramolecular chemistry remains very challenging. Here, colloidal superstructures are built and controlled using critical Casimir forces on patchy colloidal particles. These solvent-mediated forces offer direct analogues of molecular bonds, allowing patch-to-patch binding with exquisite temperature control of bond strength and stiffness. Particles with two patches are shown to form linear chains undergoing morphological changes with temperature, resembling a polymer collapse under poor-solvent conditions. This reversible temperature switching carries over to particles with higher valency, exhibiting a variety of patch-to-patch bonded structures. Using Monte Carlo simulations, it is shown that the collapse results from the growing interaction range favoring close-packed configurations. These results offer new opportunities for the active control of complex structures at the nano and micrometer scale, paving the way to novel temperature-switchable materials.

Both nature and chemistry provide many examples of molecular compounds whose structures adapt depending on changes in their environment, from the pH-dependent state of proteins to light-sensitive compounds in photochemistry. In the field of nano and microassembly, such exquisite control over structural complexity and functionality remains challenging. Still, recent progress in colloidal particle synthesis promises the assembly of complex colloidal structures, offering analogues of molecular compounds with designed structure and properties at orders of magnitude larger length scale. In particular, patchy particles promise the ability to build colloidal superstructures, opening a new route toward bottom-up structural design.[1–4] Moreover, the use of specific ligands and DNA bonding has allowed the assembly of several dedicated colloidal structures,[5,6] and depletion interaction combined with controlled surface roughness provides site-specificity.[7] Yet, a generic way to build complex superstructures and configure these structures with in situ control remains challenging.

Natural assembly processes in biology leading to complex structures often involve competing interactions, such as hydrophobic and hydrophilic interactions.[8] Indeed, simulations have shown that patchy particles interacting via hydrophobic and hydrophilic surface patches are good candidates to create desired superstructures,[4,9–12] as experimentally shown for simple two-sided Janus spheres.[13,14] Critical Casimir forces[15–17] take maximum advantage of such solvent-mediated interactions in near-critical solvents by exploiting the universal temperature dependence of solvent fluctuations to induce effective particle interactions that can be finely adjusted via the temperature-dependent solvent correlation length. Independent of whether these forces involve critical fluctuations[18] or preferential wetting,[15,16] recent research has highlighted the unique opportunities to assemble both equilibrium and out-of-equilibrium structures.[19–26] Combined with recently synthesized multivalent patchy particles,[1,27] this promises a generic way to assemble dedicated superstructures: As the Casimir force depends uniquely on the boundary conditions,[17,24,25] selective bonding should result between hydrophobic or hydrophilic particle patches, yielding specific superstructures that are analogues of molecular bonds and structures.

Here, we show that the application of critical Casimir forces on multivalent patchy particles indeed allows fine control over the assembly of colloidal superstructures. We demonstrate specific and adjustable critical Casimir bonding of hydrophobic and hydrophilic particle patches with in situ control over bond energy, range, and bond stiffness. We assemble dimer particles into colloidal analogues of molecular polymers with adjustable bending stiffness, which we measure directly from thermally activated bending fluctuations. These colloidal polymers exhibit a collapse transition close to the solvent critical point, reminiscent of molecular polymer collapse when solvent conditions change from good to poor. Using Monte Carlo simulations with an optimized potential based on experimentally measured pair correlation functions, we show that the colloidal chain collapse results from the growing interaction range due to the increasing solvent correlation length close to the solvent critical point. We demonstrate that this experimental control

Dr. T. A. Nguyen, Dr. S. J. Veen, Prof. P. Schall
Institute of Physics
University of Amsterdam
Science Park 904, Amsterdam 1098 XH, The Netherlands
E-mail: ps@peterschall.de
Dr. A. Newton, Prof. P. G. Bolhuis
Van 't Hoff Institute for Molecular Sciences
University of Amsterdam
Science Park 904, Amsterdam 1098 XH, The Netherlands
Dr. D. J. Kraft
Huygens-Kamerlingh Onnes Laboratory
Leiden University
Leiden, 2333 CA, The Netherlands

DOI: 10.1002/adma.201700819

applies also to particles with higher valence such as trimers and tetramers, allowing the assembly of even more complex, switchable structures. These results open new routes to the in situ control of nanostructures with actively controllable mechanical properties and morphologies.

We synthesize patchy particles by swelling and polymerizing clusters of polymethylmethacrylate spheres of radius $R = 1.15$ µm with a methylmethacrylate/methacrylic acid shell, resulting in geometrically well-defined patches with rotational symmetry (see the Supporting Information).[28] Hydrophobic affinity of the particle patches is achieved by grafting a polyhydroxy stearic acid-copolymer onto the patch surface. The central part of the patchy particles is made hydrophilic by using the ionic initiator potassium persulfate. These particles are dispersed in the homogeneous phase of a binary solvent of heavy water and 3-methylpyridine (3MP) at temperatures ΔT below the critical temperature $T_c = 38.55$ °C, determined by light scattering and microscopy from solvent phase separation at the critical composition. Solvents were prepared with 3MP weight fractions $c_{3MP} = 0.25$ and 0.31, slightly to the left and right of the critical composition $c_c = 0.28$,[29] respectively. Due to their hydrophobicity, the particle patches have strong affinity for the nonaqueous component (3MP) of the binary solvent, while the hydrophilic shells have affinity for water. When approaching the critical temperature from below, the homogeneous solvent shows increasing composition fluctuations. Confined in the liquid gap between the particle surfaces, these composition fluctuations give rise to a Casimir-like force[30] known as the critical Casimir force. Because strong critical Casimir forces arise in solvents poor in the component preferred by the particle surfaces,[31–33] this should lead to binding of the hydrophobic patches in 3MP-poor, and of the hydrophilic shells in 3MP-rich solvents, see **Figure 1**a,b.

Indeed we observe that in solvents with concentrations $c_{3MP} < c_c$ the particle patches approach each other at temperatures close to T_c, and dimer particles assemble into directed, chain-like structures as shown in Figure 1c. By contrast, in 3MP-rich solvents, the particles approach each other sideways resulting in distinct parallel structures (Figure 1d). This site-specific interaction leads to increasingly complex structures for higher-valency particles, as shown in Figure 1g–l, where we display trimer particles interacting in the same solvents as before. Here, the patch-to-patch binding in 3MP-poor solvents leads to staggered chains (Figure 1i,k), while the side-by-side binding in 3MP-rich solvents leads to bent filaments associated with the dense alternating stacking of trimers (Figure 1j,l). In all cases, the assembly is fully reversible as confirmed by the break-up of aggregates upon lowering the temperature several degrees below T_c. This specific bonding can be further tuned by varying the patch width: using particles with narrower patches, we observe that bond angles narrow, and the bonding becomes even more specific, in agreement with simulation predictions,[34] as shown in Figure S1 in the Supporting Information. We hence achieve specific, reversible critical Casimir interactions associated with the surface-specific adsorption preferences that set the boundary conditions of the critical Casimir force.

The advantage of the critical Casmir interaction is that we can in situ control the magnitude and range of the site-specific

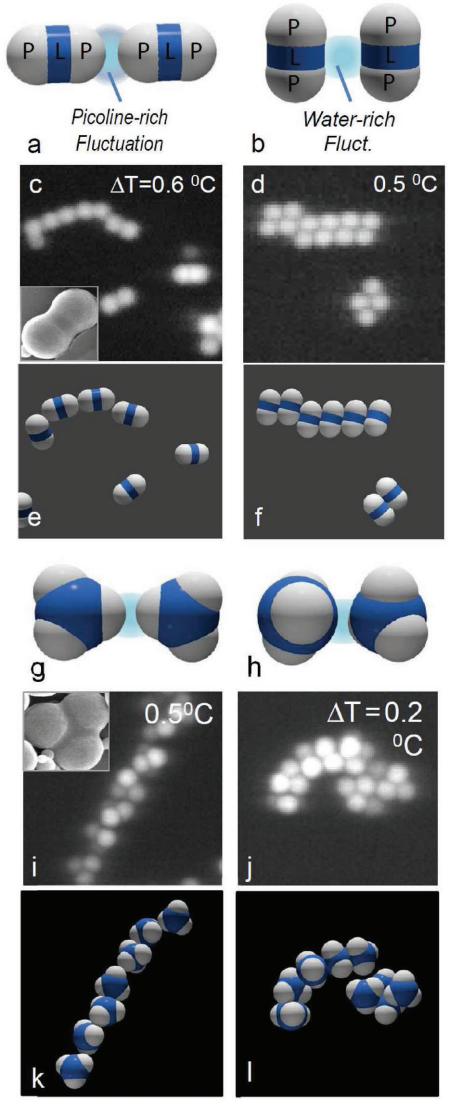

Figure 1. Bonding of dimer and trimer particles by critical Casimir forces. a–f) Bonding of dimer particles in 3MP-poor (left) and 3MP-rich solvents (right). a,b) Principle of the specific critical Casimir interaction: 3MP-rich fluctuations confined between hydrophobic patches (*P*) cause patch-to-patch binding for solvent compositions $c_{3MP} < c_c$ (a), while water-rich fluctuations confined between hydrophilic shells (*L*) lead to shell-to-shell binding for solvent compositions $c_{3MP} > c_c$. (b). c,d) Confocal microscope images and e,f) schematic of resulting particle configurations. Chain-like structures in solvents with $c_{3MP} = 0.25 < c_c$ demonstrate patch-to-patch binding (c,e), while parallel structures in solvents with $c_{3MP} = 0.31$ demonstrate sideways attraction (d,f). The inset in panel (c) shows scanning electron microscope (SEM) image of dimer particle. g–l) Bonding of trimer particles in 3MP-poor (left) and 3MP-rich solvents (right): schematic (g,h), confocal microscope images (i,j) and schematic of particle configurations (k,l). Staggered chains indicate patch binding (i,k), while curled filaments indicate shell binding (j,l).

attraction, thereby changing the bond and bending stiffness of the structures. We focus on dimer particles and measure the bond stiffness directly from thermal fluctuations in the positions and alignment of bonded dimer pairs. For each temperature, we record several thousand images of particle configurations to determine distances between neighboring

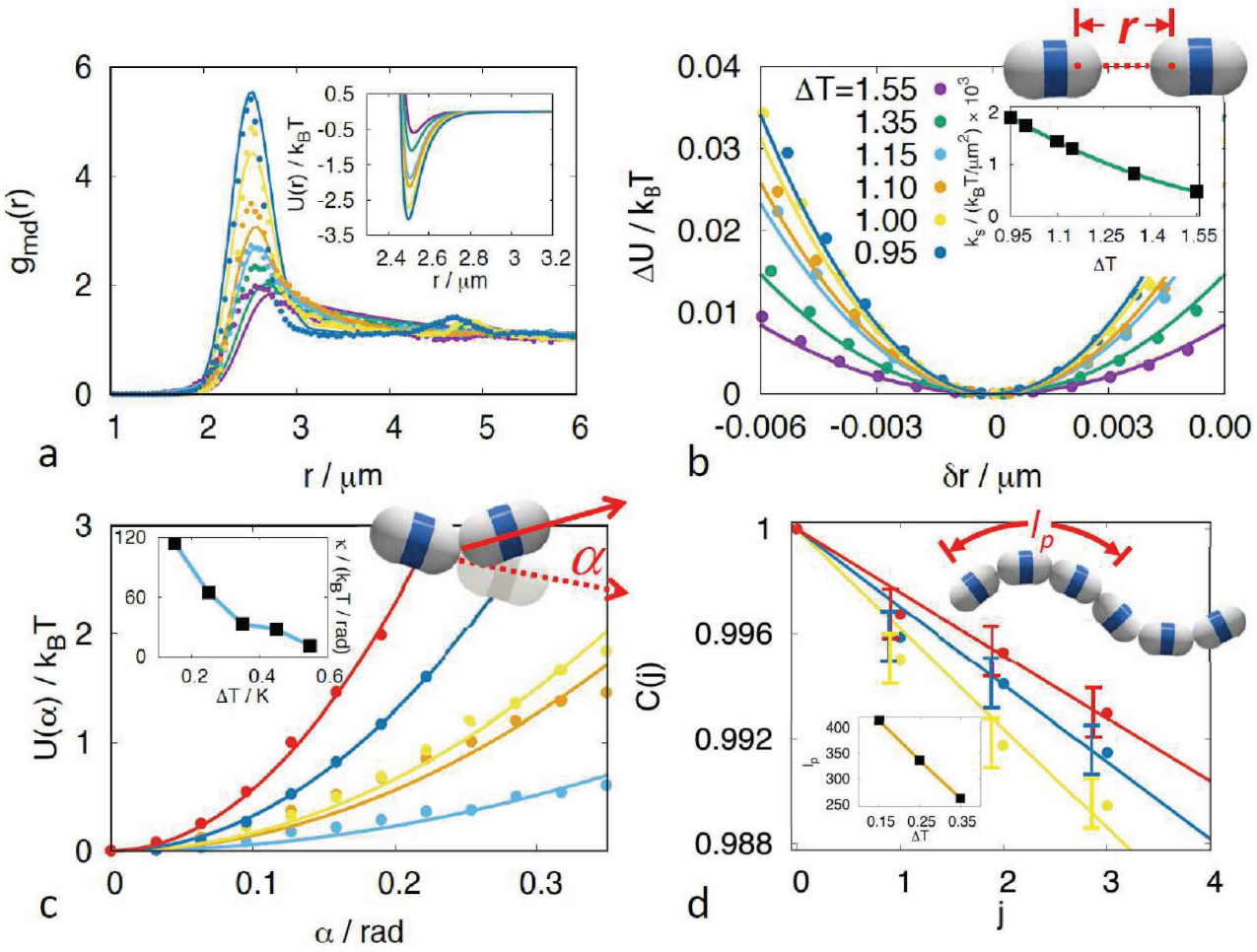

Figure 2. Adjustable bond and bending stiffness. a) Particle pair potential, b) bond stretching, and c) bending stiffness, and d) chain bending stiffness for various temperatures ΔT at solvent composition $c_{3MP} = 0.25$. a) Nearest-neighbor pair correlation function for $\Delta T = 1.55$ (purple), 1.35 (green), 1.15 (light blue), 1.10 (orange), 1.0 (yellow), and 0.95 (dark blue), showing good agreement between experiment (dots) and simulation (curves). The inset: derived optimized pair potentials. b) Bond stretching potentials as a function of the deviation δr from the potential minimum as obtained from the optimized potentials in panel (a) (points) and quadratic fits (curves). The inset: resulting bond stretching spring constant as a function of ΔT. c) Measured bending potential as a function of bending angle α obtained from bond angle distributions $p(\alpha)$ using $p(\alpha) \propto \exp(-U(\alpha)/kT)$, for $\Delta T = 0.55$ (light blue), 0.45 (orange), 0.35 (yellow), 0.25 (dark blue), and 0.15 (red). Solid lines indicate harmonic fits. The inset: resulting bending stiffness as a function of ΔT. d) Chain orientational correlation function versus particle distance along the chain. Due to high chain stiffness, the correlation function decays only little for a few particles, and the exponential decay is approximated by a straight line. The persistence length and corresponding bending stiffness increase with the increasing critical Casimir interactions upon approaching T_c, see the inset.

particle centres in the form of radial distribution functions (see **Figure 2**a). These distributions are broadened by particle polydispersity and locating inaccuracies; to find the pair potential, we therefore used simulations to predict pair correlation functions based on an effective pair potential model, and determined those that best match the measured distributions. We use a divalent particle model consisting of two fused spheres (patches) of radius R interacting via effective attractive pair potentials as introduced in ref. [35] In principle also repulsive critical Casimir forces act between unlike parts of the dimer particle, which we account for only implicitly by the choice of fitting parameters below. Furthermore, while for spherical particles, more exact models for critical Casimir interactions are available,[19,23] we find that this simple model provides a good approximation at the relevant (large) particle surface distances.[36] The patch–patch potential is assumed to be isotropic and determined by a balance of a repulsive screened electrostatic potential and a solvent-mediated attractive Casimir potential according to $U = U_{el} - U_{Cas}$, where $U_{el} = A_{el} \exp[-(r - 2R)/l_D]$ and $U_{Cas} = A_{Cas}\exp[-(r - 2R)/\xi]$, with r the separation of the centres of two spheres not belonging to the same dumbbell, $A_{el} = (2\pi R\sigma_c^2 l_D^2)/(\varepsilon\varepsilon_0)$ the strength of the electrostatic repulsion, A_{Cas} the amplitude of the critical Casimir force and the solvent correlation length $\xi = \xi(c_{3MP},\Delta T)$ that depends on both solvent composition and temperature. For our solvents close to the critical composition, we use the simplified scaling $\xi = \xi_0(\Delta T/T_c)^{-0.63}$ of the critical composition, which for temperatures $\Delta T \geq 1$ °C is within 5% of the actual off-critical correlation length.[37] We also neglect Van der Waals forces that are not important for the observed reversible assembly. Using

the surface charge $\sigma_C = -0.188$ μC cm^{-2} measured by electrophoresis, and the Debye screening length $l_D = 24$ nm determined by conductivity measurements, the electrostatic repulsion is known, and the only free parameters are the amplitude A_{Cas} and correlation length ξ_0 far away from the critical point.

As shown in Figure 2a, we obtain a good fit of the measured pair correlations for $\xi_0 = 1.6$ nm, larger than typical literature values of around 0.3 nm[38] but in agreement with a recent value of 1.5 nm used in the modeling of critical Casimir potentials,[33] and $A_{Cas} = 2\pi R/\xi$, the amplitude at the critical composition, which is smaller than the expected off-critical amplitude, likely reflecting the complex particle geometry. The resulting pair potential (the inset) becomes deeper and longer-ranged upon approaching T_c as expected. In analogy to molecular bonds, this increasing potential depth is associated with an increasing bond stiffness, which we illustrate by plotting the potential energy with respect to the minimum, $\Delta U = U - U_0$, versus the stretching from the equilibrium separation, δr, in Figure 2b. To extract the stretching stiffness, we fit the data with a quadratic function on the left side of the minimum; at larger distances, higher-order (anharmonic) contributions lead to deviations from harmonic behavior, similar to molecular potentials. The extracted spring constant increases with decreasing ΔT due to the increasing critical Casimir force, see the inset of Figure 2b. We also measure the bending stiffness from thermal fluctuations of the bond angles. At low attraction where bonds break up frequently, the bond is entirely flexible and shows barely any stiffness against bending deformations. In contrast, at higher attraction ($\Delta T < 0.5$ °C), the distribution of bond angles $p(\alpha)$ narrows, and we can directly infer the bending potential $U(\alpha)$ using $p(\alpha) \propto \exp(-U(\alpha)/kT)$. The resulting bending potential shown in Figure 2c clearly increases more steeply at smaller ΔT, indicating increasing bending stiffness. This is confirmed when we plot the bending stiffness, κ, determined from quadratic fits as a function of ΔT in Figure 2c, inset.

The increasing bond stiffness leads to an increasing persistence of the assembled chain against bending deformations. We measure the corresponding persistence length directly from fluctuations in the orientations of the chain elements. Correlated fluctuations decay over the persistence length l_p that is directly related to the bending stiffness κ via $l_p = 2a\kappa/k_B T$, assuming a worm-like chain model in two dimensions.[39] Here $a = 4.6$ μm is the length of a single dimer particle. We follow the assembled dimer particles over time, and determine correlations in the fluctuations of their orientations. We find indeed increasing correlations upon approaching T_c, indicating increasing bending rigidity of the chain as shown in Figure 2d. Due to the high chain stiffness, the bending correlations decay only little; we can nevertheless estimate a corresponding effective persistence length increasing from $\approx 250a$ at $\Delta T = 0.35$ °C to $\approx 400a$ at $\Delta T = 0.15$ °C, indicating a bending stiffness increasing from 125 to 200 $k_B T$, respectively, which is indeed within the same order of magnitude as the directly measured bending stiffness in Figure 2c. Hence, we can adjust the chain stiffness by changing the critical Casimir bond strength via temperature. This rather high stiffness is not present in the effective potential model, and we associate it with surface friction effects of the polymer-coated patches, which restrict the orientational degrees of freedom of the dimer particles with respect to the freely joint case.

Nevertheless, the bending fluctuations allow the chain to sample different conformational states, thus contributing to its conformational entropy. Strikingly, upon further approaching T_c, we observe that the chain spontaneously collapses into a compact state, as shown by the time evolution of the structure after a jump to $\Delta T = 0.05$ °C in **Figure 3**a. The dimer particles approach each other sideways, and eventually form a close-packed arrangement. In this close-packed state, a particle has more bonding neighbours, and hence larger bond energy. The observed collapse transition is reminiscent of a polymer collapse occurring when solvent conditions go from good to poor. Also here the reduction of chain conformational entropy is offset by the stronger interparticle energy. Using our approximate pair potential, we can qualitatively model the collapse transition using dynamical Monte Carlo simulations that start from quenched networks, and subsequently relax these configurations by increasing the temperature and hence the interaction strength and range (see the Supporting Information). Figure 3c shows that indeed a qualitatively similar collapse transition occurs when the correlation length becomes sufficiently large close to T_c. The figure shows dynamical Monte Carlo snapshots during relaxation from the quenched network. The extrapolated potentials for the experimental temperature range $\Delta T < 0.5$K are shown in Figure 3d. For temperatures close to T_c, the potential becomes longer ranged but also shallower, a consequence of the $1/\xi$ dependence of the Casimir interaction that is confirmed in field-theoretical models.[33] The longer range together with the shallower effective potential drives the collapse into the compact state. Indeed we find that close to T_c, the resulting interaction energy per particle increases from three to five times the potential depth due to the interaction with more neighbors (Figure 3e), hence clearly indicating the bond energy gain. We note, however, that close to the critical temperature, the assumed scaling of the correlation length is no longer accurate and our simplified model breaks down. At $\Delta T \approx 0.05$ °C for example, the correlation length for this off-critical composition is around three times smaller than the value at the critical composition, as shown by recent detailed measurements and modeling.[37] Furthermore, many-body effects may become important for such extended correlations, violating the assumed pairwise additivity.[20,36,40] Nevertheless, the temperature $\Delta T \approx 0.05$ °C at which this interaction energy increase starts to happen agrees surprisingly well with our observations of the collapse. We further observe that similar collapses occur for higher-order multipole particles such as trimers and tetramers (see the Supporting Information), demonstrating the generality of this phenomenon. Interestingly, the collapse is also reversible: we observe that collapsed aggregates open again when we reduce the temperature away from T_c though on longer timescales, as shown in Figure 3b, indicating that this collapse happens indeed close to equilibrium.

Tunable site-specific critical Casimir interactions provide novel control to assemble complex colloidal superstructures. Their temperature dependence offers direct in situ adjustment of the bond stiffness, allowing the mechanical properties of the assembled structure to be tailored and switched between different morphological states. We have demonstrated this new

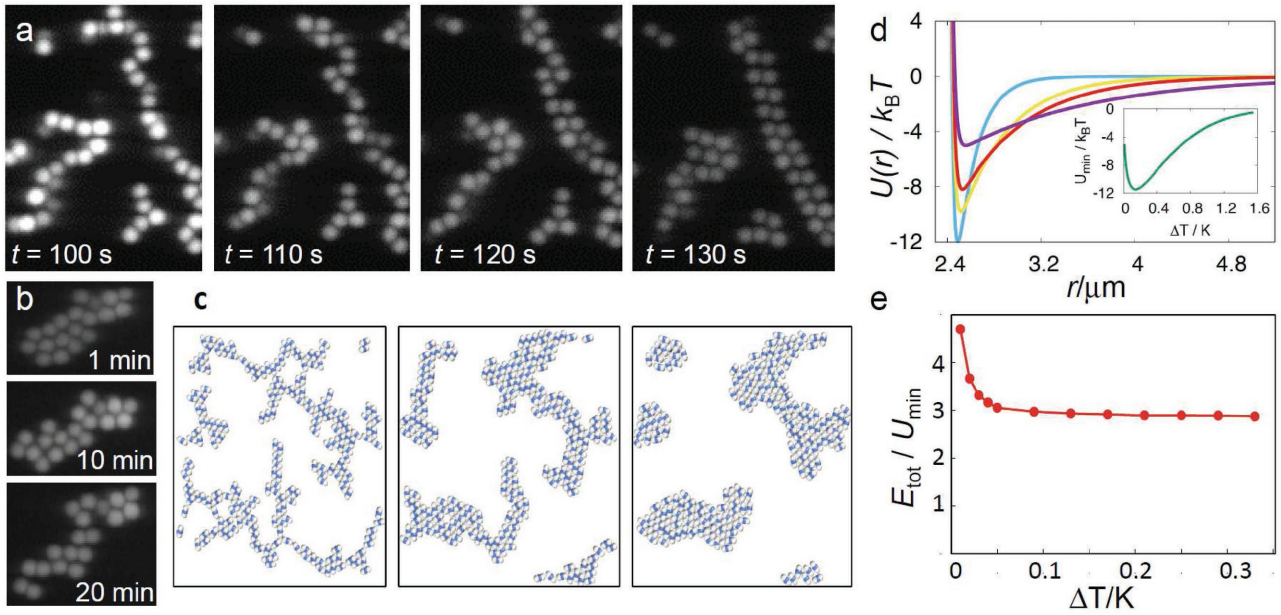

Figure 3. Observation of chain collapse. a) Time evolution of dimer particle chains after temperature change from $\Delta T = 0.1$ to $\Delta T = 0.05$ °C at solvent composition $c_{3MP} = 0.25$. The chains collapse into denser structures, in which particles have more bonds. b) Slow reopening of the collapsed dimer particle chain upon increasing ΔT. c) Dynamic Monte Carlo simulation of chain collapse. Snapshots are obtained during relaxation at $\Delta T = 0.01$ corresponding to $\xi = 1.1$ μm. The structure relaxes to a compact configuration as the pair potential becomes longer ranged and also shallower. d) Extrapolated optimized pair potentials for $\Delta T = 0.20$ (light blue), 0.05 (yellow), 0.03 (red), and 0.01 °C (purple). The inset shows the nonmonotonic behavior of the potential well depth as a function of ΔT. e) Average energy per particle normalized to the potential well depth as a function of ΔT in the relaxed structure. Below $\Delta T \approx 0.05$ K, the number of bonds with neighboring particles increases from 3 to 5.

control for dimer particles forming chains that resemble molecular polymers. By adjusting the strength and range of the patchy interaction, we varied the chain's bending rigidity, and induced collapses into compact states resembling molecular polymer collapse. Besides DNA bonding and depletion interaction on anisotropic particles, for which temperature dependence can be in principle introduced using temperature-dependent depletant, our system offers an effective, solvent-mediated interaction that implicitly depends on temperature in a universal way. Application to higher-valency particles allows the formation of more complex superstructures, with in situ control over their mechanical properties and structural morphology. This principle introduces flexibility and responsiveness into complex assembled colloidal structures on the way to analogues of molecular compounds. Because statistical mechanics dictates the equilibrium structure as the one exhibiting the lowest free energy, in analogy to molecular structures, this opens the door to the design of complex colloidal superstructures through fine control of patchy particle interactions.

Supporting Information

Supporting Information is available from the Wiley Online Library or from the author.

Acknowledgements

This work was supported by the Foundation for Fundamental Research on Matter (FOM), which is subsidized by the Netherlands Organization for Scientific Research (NWO), and by a Vici grant from NWO.

Conflict of Interest

The authors declare no conflict of interest.

Keywords

colloidal assembly, critical Casimir effect, nanoassembly, patchy colloids

Received: February 9, 2017
Revised: June 9, 2017
Published online: July 10, 2017

[1] V. N. Manoharan, M. T. Elsesser, D. J. Pine, *Science* **2003**, *301*, 483.
[2] S. C. Glotzer, M. J. Solomon, *Nat. Mater.* **2007**, *6*, 557.
[3] S. Sacanna, D. J. Pine, *Curr. Opin. Colloid Interface Sci.* **2011**, *16*, 96.
[4] F. Smallenburg, F. Sciortino, *Nat. Phys.* **2013**, *9*, 554.
[5] Y. Wang, Y. Wang, D. R. Breed, V. N. Manoharan, L. Feng, A. D. Hollingsworth, M. Weck, D. J. Pine, *Nature* **2012**, *491*, 51.
[6] W. Liu, M. Tagawa, H. L. Xin, T. Wang, H. Emamy, H. Li, K. G. Yager, F. W. Starr, A. V. Tkachenko, O. Gang, *Science* **2016**, *351*, 582.
[7] D. J. Kraft, R. Ni, F. Smallenburg, M. Hermes, K. Yoonc, D. A. Weitz, A. van Blaaderen, J. Groenewold, M. Dijkstra, W. K. Kegel, *Proc. Natl. Acad. Sci. USA* **2012**, *109*, 10787.
[8] P. Nelson, *Biological Physics, Energy, Information, Life*,W. H. Freeman and Company, New York **2004**.
[9] E. Bianchi, J. Largo, P. Tartaglia, E. Zaccarelli, F. Sciortino, *Phys. Rev. Lett.* **2006**, *97*, 168301.
[10] E. Bianchi, P. Tartaglia, E. Zaccarelli, F. Sciortino, *J. Chem. Phys.* **2008**, *128*, 144504.
[11] W. L. Miller, A. Cacciuto, *Phys. Rev. E* **2009**, *80*, 021404.

[12] G. Doppelbauer, E. Bianchi, G. Kahl, *J. Phys.: Condens. Matter* **2010**, *22*, 104105.
[13] Q. Chen, J. K. Whitmer, S. Jiang, S. C. Bae, E. Luijten, S. Granick, *Science* **2011**, *331*, 199.
[14] C. Yu, J. Zhang, S. Granick, *Angew. Chem.* **2014**, *53*, 4364.
[15] D. Beysens, D. Estève, *Phys. Rev. Lett.* **1985**, *54*, 2123.
[16] M. E. Fisher, P. G. de Gennes, *C. R. Seances Acad. Sci., Ser. B* **1978**, *287*, 207.
[17] C. Hertlein, L. Helden, A. Gambassi, S. Dietrich, C. Bechinger, *Nature* **2008**, *451*, 172.
[18] A. Hanke, F. Schlesener, E. Eisenriegler, S. Dietrich, *Phys. Rev. Lett.* **1998**, *81*, 1885.
[19] A. Gambassi, A. Maciołek, C. Hertlein, U. Nellen, L. Helden, C. Bechinger, S. Dietrich, *Phys. Rev. E* **2015**, *80*, 061143.
[20] J. R. Edison, N. Tasios, S. Belli, R. Evans, R. van Roij, M. Dijkstra, *Phys. Rev. Lett.* **2015**, *114*, 038301.
[21] V. D. Nguyen, S. Faber, Z. Hu, G. H. Wegdam, P. Schall, *Nat. Commun.* **2013**, *4*, 1584.
[22] P. B. Shelke, V. D. Nguyen, A. V. Limaye, P. Schall, *Adv. Mater.* **2013**, *25*, 1499
[23] T. F. Mohry, A. Maciołek, S. Dietrich, *J. Chem. Phys.* **2012**, *136*, 224902.
[24] F. Soyka, O. Zvyagolskaya, C. Hertlein, L. Helden, C. Bechinger, *Phys. Rev. Lett.* **2008**, *101*, 208301.
[25] a) M. Tröndle, S. Kondrat, A. Gambassi, L. Harnau, S. Dietrich, *Europhys. Lett.* **2009**, *88*, 40004; b) A. Gambassi, S. Dietrich, *Soft Matter* **2011**, *7*, 1247.
[26] V. D. Nguyen, M. T. Dang, T. A. Nguyen, P. Schall, *J. Phys.: Condens. Matter* **2016**, *28*, 043001.
[27] D. J. Kraft, W. S. Vlug, C. M. van Kats, A. van Blaaderen, A. Imhof, W. K. Kegel, *J. Am. Chem. Soc.* **2008**, *131*, 1182.
[28] M. T. Elsesser, A. D. Hollingsworth, K. V. Edmond, D. J. Pine, *Langmuir* **2011**, *27*, 917.
[29] J. D. Cox, *J. Chem. Soc.* **1952**, *897*, 4606.
[30] H. B. G. Casimir, *Proc. K. Ned. Akad. Wet., Ser. B* **1948**, *51*, 793.
[31] P. D. Gallagher, J. V. Maher, *Phys. Rev. A* **1992**, *46*, 2012.
[32] O. A. Vasilyev, S. Dietrich, *Europhys. Lett.* **2013**, *104*, 60002.
[33] T. F. Mohry, S. Kondrat, A. Maciolek, S. Dietrich, *Soft Matter* **2014**, *10*, 5510.
[34] A. Giacometti, F. Lado, J. Largo, G. Pastore, F. Sciortino, *J. Chem. Phys.* **2010**, *132*, 174110.
[35] a) D. Bonn, J. Otwinowski, S. Sacanna, H. Guo, G. H. Wegdam, P. Schall, *Phys. Rev. Lett.* **2009**, *103*, 156101; b) A. Gambassi, S. Dietrich, *Phys. Rev. Lett.* **2010**, *105*, 059601; c) D. Bonn, G. H. Wegdam, P. Schall, *Phys. Rev. Lett.* **2010**, *105*, 059602.
[36] M. T. Dang, A. Vila Verde, P. G. Bolhuis, P. Schall, *J. Chem. Phys.* **2013**, *139*, 094903.
[37] S. G. Stuij, M. Labbé-Laurent, T. E. Kodger, A. Maciolek, P. Schall, *Soft Matter* **2017**, DOI: 10.1039/c7sm00599g.
[38] P. K. Madhavan Unni, *J. Chem. Phys.* **2006**, *124*, 054505.
[39] L. D. Landau, E. M. Lifshitz, *Theory of Elasticity*, Pergamon, New York **1986**.
[40] S. Paladugu, A. Callegari, Y. Tuna, L. Barth, S. Dietrich, A. Gambassi, G. Volpe, *Nat. Commun.* **2016**, *7*, 114003.

